

Accepted Manuscript

Title: Pd/C modified with Sn catalyst for liquid-phase selective hydrogenation of maleic anhydride to gamma-butyrolactone

Authors: Rongrong Li, Jia Zhao, Deman Han, Xiaonian Li

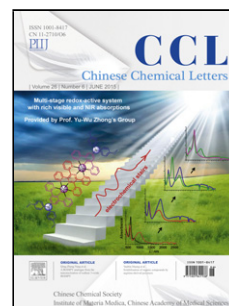
PII: S1001-8417(17)30165-1
DOI: <http://dx.doi.org/doi:10.1016/j.ccllet.2017.04.028>
Reference: CCLET 4064

To appear in: *Chinese Chemical Letters*

Received date: 3-2-2017
Revised date: 5-3-2017
Accepted date: 23-4-2017

Please cite this article as: Rongrong Li, Jia Zhao, Deman Han, Xiaonian Li, Pd/C modified with Sn catalyst for liquid-phase selective hydrogenation of maleic anhydride to gamma-butyrolactone, *Chinese Chemical Letters* <http://dx.doi.org/10.1016/j.ccllet.2017.04.028>

This is a PDF file of an unedited manuscript that has been accepted for publication. As a service to our customers we are providing this early version of the manuscript. The manuscript will undergo copyediting, typesetting, and review of the resulting proof before it is published in its final form. Please note that during the production process errors may be discovered which could affect the content, and all legal disclaimers that apply to the journal pertain.



Original article

Pd/C modified with Sn catalyst for liquid-phase selective hydrogenation of maleic anhydride to gamma-butyrolactone

Rongrong Li ^{a, b}, Jia Zhao ^a, Deman Han ^{b, *}, Xiaonian Li ^{a, **}^a Industrial Catalysis Institute of Zhejiang University of Technology, Hangzhou 310014, China^b School of Pharmaceutical and Chemical Engineering, Tai Zhou University, Taizhou 317000, China

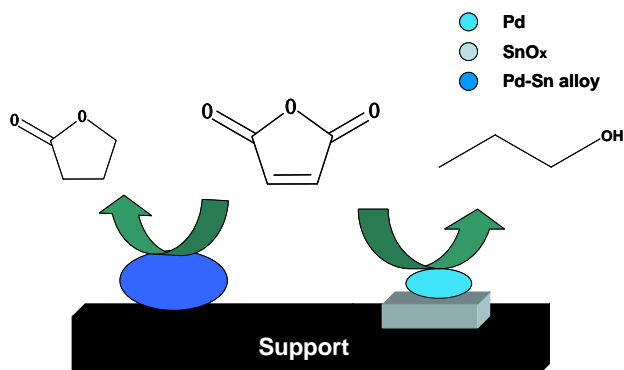
* Corresponding author.

E-mail address: hdm@tzc.edu.cn (Deman Han).

** Corresponding author.

E-mail address: xnli@zjut.edu.cn (Xiaonian Li).

Graphical Abstract



The types of alloy phase and the amounts of the surface Pd-SnO(*x*) sites altered along with Sn/Pd mass ratios from 0–1.0 synthesized in the process of preparation. The maximum reaction rate was 0.57 mol-GBL/(mol-Pd·min) and selectivity was 95.94% when the Sn/Pd mass ratio was 0.6. It might be attributed to the formation of Pd₂Sn alloy and less amounts of Pd-SnO(*x*) sites.

ABSTRACT

Pd catalysts suffered from poor selectivity and stability for liquid-phase hydrogenation of maleic anhydride (MA) to gamma-butyrolactone (GBL). Thus, Pd/C catalysts modified with different Sn loadings were synthesized, and characterized by XRD, XPS, TEM and elemental mapping. The types of alloy phase and the amounts of the surface Pd-SnO(*x*) sites altered along with Sn/Pd mass ratios from 0–1.0 synthesized in the process of preparation. The maximum reaction rate was 0.57 mol-GBL/(mol-Pd·min) and selectivity was 95.94% when the Sn/Pd mass ratio was 0.6. It might be attributed to the formation of Pd₂Sn alloy and less amounts of Pd-SnO(*x*) sites.

Keywords:

Bimetallic catalysts

Sn/Pd mass ratio

Maleic anhydride
Selective hydrogenation
Gamma-butyrolactone

1. Introduction

Gamma-butyrolactone (GBL) has been widely used in the manufacture of substituted pyrrolidones, agrochemicals, pharmaceuticals, biodegradable polymers and paint industries [1-5]. Directly selective hydrogenation of maleic anhydride (MA) into GBL should be a friendly environmental method, although homogeneous Ru catalysts still is of low activity and difficult separation [6, 7] and heterogeneous Cu [8-13] or Ni [14-17] suffers from low activity and poor selectivity to GBL. Moreover, some bimetallic catalysts, such as Cu-Cr, were undesirable due to their high toxicity [18]. Palladium is one of the most versatile elements in catalysis [19-23], and recently S. Jung et al. [33] reported that addition of Sn to Pd/SiO₂ catalysts could increase the selectivity remarkably in hydrogenation of MA to GBL. However, the literatures concerning the interaction of Pd-Sn for selective hydrogenation reaction were limited [30-32].

In this work, the Pd/C catalysts modified with different Sn loadings were synthesized, and characterized by XRD, XPS, TEM and elemental mapping. The catalysts have been tested on a laboratory scale plant for the selective hydrogenation of MA to GBL under the relative mild reaction conditions, discussing the improvement of Sn to the hydrogenation activity and selectivity of Pd/SiO₂. The experimental results illustrated that the surface composition of Pd-Sn nanoparticles plays an essential role for this hydrogenation reaction, and the PdSn/C catalyst with nominal mass ratio 0.6 of Sn/Pd shows good activity and high selectivity in the hydrogenation of MA to GBL.

2. Results and discussion

The XRD patterns of the PdSn(*x*) catalysts are shown in Fig. 1(a) and the corresponding magnified peaks are exhibited in Fig. 1(b). No SnO_x was observed in the XRD patterns of reduced samples in H₂ stream at 723 K. The (111) facet of the Pd patterns at the Bragg peak of 40.2 ° has been affiliated to a vertical line in Fig. 1. The presence of metallic Pd phase could be observed even mainly diffraction peaks overlapping with the XRD-peaks of Pd-Sn phase. Obviously, Fig. 1(a) demonstrated that a transformation has taken place since the samples with different Sn/Pd mass ratios result in different Pd-Sn alloy phase. Pd₃Sn, Pd₂Sn and Pd₃Sn₂ phases were detected corresponding to PdSn(0.2), PdSn(0.6) and PdSn(1.0) samples, respectively. Furthermore, it could be observed that the main diffraction peak of all the Pd-Sn NPs catalysts were located at lower 2θ values with respect to the corresponding peaks of the Pd NPs. The atomic radius of Pd (1.79 Å) and Sn (1.72 Å) were extremely close, so that the a small amount shift in position with respect to (111) facet of Pd could be possible due to the lattice contraction arising from the incorporation of the smaller Sn atoms into the Pd lattice, suggesting the Pd-Sn alloy was occurred [34, 35]. It was noted that the change in the average crystallite size of the Pd-Sn NPs was not accompanied with linearly increase with Sn/Pd mass ratios, while PdSn(0.6) sample (111) facet diffraction peak was obviously much broader than others, demonstrating that the Pd and Sn species in this sample are more highly dispersive. The crystal structure of the alloy particles seemed practical equally with increasing Sn/Pd mass ratios, while incremental Sn/Pd mass ratios had almost no effect on the alloy crystal structures [36].

Fig. 2 presented the TEM images of low resolution and high resolution and their corresponding particle size distribution histograms of the PdSn catalysts. The results showed a significant difference in surface morphology with different Sn/Pd mass ratios. Although, the Pd-Sn NPs were well dispersed on the surface of support, the size distribution of particles was more pronounced for the PdSn(0.6) sample, of which the mean particle size was about 4.6 ± 0.7 nm and the distribution of particle size shifted to a narrower

region. The corresponding particle size of the PdSn(0.2) sample has shifted to 4–13 nm range and the mean particle sizes was about 8.9 ± 0.9 nm. Nevertheless, the mean particle size will reach to 12.3 ± 0.8 nm by the addition of Sn/Pd mass ratio. Thus, it appeared that the presence of Sn at PdSn(0.2) and PdSn(1.0) samples could induce the sintering or agglomeration of Pd. The high-resolution transmission electron microscopy (HRTEM) image also confirmed that the existing of Pd-Sn alloy during the preparing of the PdSn(*x*) catalysts. As red-circled indicated in Fig. 2(a-2) and (b-2), only one lattice plane illustrated the NPs, of which the spacings of inter-plane were 0.2256 and 0.2290 nm corresponding to the (110) plane of Pd₃Sn and (301) plane of Pd₂Sn type alloys, respectively. Furthermore, as red-circled presented in Fig. 2(c-2), two kinds of lattice planes illustrated the NPs. The spacing of inter-plane was 0.2208 nm affiliated to the (110) plane, and the 0.2270 nm was affiliated to the (102) plane of Pd₃Sn₂. These results were well matched with previous XRD results.

The elemental mapping analysis of Pd-Sn NPs within a randomly selected area directly confirmed that the formation of Pd-Sn alloy took place on those samples. As can be seen, the PdSn(0.2) catalyst had remarkably larger particles (~10 nm) on the carbon support, and many Pd elemental signals aggregated while Sn signals displayed uniformly (Fig. 3a), comparatively. However, we found that small particles size (~5 nm) showed on the PdSn(*x*) catalysis which was also confirmed by an HRTEM characterization (Fig. 2b). Elemental mapping analysis showed that Pd and Sn signals were presented uniformly, and the two kinds of metal particles were equally distributed and had close interaction (Fig. 3b). When the Sn/Pd mass ratio further increased to 1.0, the larger Pd-Sn alloy particles were found to be predominant in the diameter range of 4–20 nm (Fig. 3c), while the mapping analysis could unambiguously displayed that Sn and Pd elements appeared relatively homogenous and uniform distribution, which further emphasized the formation of Pd-Sn alloy and larger Pd-Sn alloy nanoparticles might be possible due to the growing up of alloy at such concentrations. Consequently, it appears that a better Pd dispersion on the support of carbon by additional inducing of Sn, and increasing of Sn/Pd mass ratio at low ratios could efficiently prevent the sintering or agglomeration of Pd, while further increasing of Sn/Pd mass ratio may result in the growing-up alloy with larger NPs size.

X-ray photoelectron spectroscopy (XPS) measurements were performed on PdSn(*x*) catalysts to determine the surface, near-surface composition and the surface states of various species. The XP spectra of the Pd 3d and Sn 3d are presented in Fig. 4(a) and (b), respectively, and the results of the XPS investigations are collected in Table 1.

In Fig. 4(a), as we can see, there is a significant difference with binding energy (BE) for PdSn(*x*) catalysts when examining the Pd 3d spectra. Two different Pd species were detected with BE at 335.3–335.8 and 336.7–337.4 eV, which were associated with the metallic Pd effects and Pd species, respectively, due to the formation of Pd-Sn intermetallic compounds [37, 38]. Thus, on the surface regions of the sample, two different kinds of Pd were presented: isolated one and the alloy phase. About 46.5% of surface Pd atoms were intermetallic state for the PdSn(0.2) sample. The formation of Pd₃Sn was also illustrated by XRD peaks in Fig. 2. It should be noted that even for the metallic Pd, the BE is still 0.2–0.3 eV higher than pure Pd [37–40]. The Pd binding energy shifted upward which could be illustrated by the presence of a Pd-Sn alloy [41, 42] and an electron transfer from Sn to Pd might occur [43]. The XP spectra for PdSn(0.6) and PdSn(1.0) samples in Fig. 4(a) there are two characteristic peaks ascribed to metallic palladium and intermetallic palladium, respectively. In addition, it was found that the value for Pd 3d significantly increased from 335.3 to 335.7 and 335.8 eV along with the increase of the Sn/Pd ratios from 0.2 to 0.6 and 1.0, respectively. By the FWHM (full width of at half-maximum), considering the results presented in Table 1, the formation of more than one palladium species was observed since FWHM of the Pd peak is much more larger [44]. However, from Table 1, it was worth noting that content of Pd in intermetallic state was not changed too much for the PdSn(0.6) (45%) and PdSn(1.0) (44%), in comparison with the PdSn(0.2) (46%) in the intermetallic form.

XPS measurements illustrated the formation of metallic Sn in the as-prepared Pd-Sn catalysts, meanwhile the proportion of reduced Sn increased with Sn/Pd mass ratios. According to Fig. 4(b), three distinguished peaks at about 485.3, 486.6 and 487.5 eV (left to right) illustrated the metallic Sn, Sn²⁺ (phases of Pd-Sn-O and/or Sn-O), and Sn⁴⁺ peak positions for Sn 3d_{5/2} core levels, respectively. In addition, Table 1 exhibited the proportion of oxidized states tin species in Pd-Sn/C decreasing from 85% to 76% and 72% for the PdSn(0.2), PdSn(0.6) and PdSn(1.0) samples, respectively. While considering the loading of Sn increased from 1% to 3% and 5%, the oxidized states tin species still increased from 0.85% to 2.28% and 3.60% in mass loading, respectively.

The catalytic activities and selectivity with different Sn/Pd mass ratios were presented in Table 2. The rate of reaction broadly ranged from 0.03 to 0.57 mol-GBL/(mol-Pd·min) for the different Sn/Pd mass ratios Pd-Sn/C bimetallic catalysts.

As we can see, during MA hydrogenation, the reaction rate became faster for the Sn-containing catalysts. The catalytic activity was improved by addition of Sn to Pd forming Pd-Sn alloy NPs. However, the catalytic activity was decreased at the Sn/Pd mass ratio 1.0. As expected, the PdSn(0.6) sample was more active for the MA hydrogenation to GBL. Interestingly, the GBL selectivity performance in the same trend as the activity mentioned above. The GBL selectivity could be reached at 95.94% for the PdSn(0.6) catalyst.

The main by-product in the process of reaction was *n*-butyl alcohol (NBA), and the percentages of other by-products were small as shown in Table 2. The succinic anhydride (SAH) was only appeared when using Pd/C catalyst, while for the Sn-containing catalysts SAH was not observed at high conversion levels. The NBA selectivity decreased with the increased Sn/Pd mass ratios, and reached a minimum when Sn/Pd mass ratio was 0.6. However, the NBA selectivity increased when the Sn/Pd mass ratios further increased, almost equally to that of monometallic Pd/C catalyst.

In order to investigate the reasons for the high yield of NBA, the controlled experiments for the prepared Pd/SnO₂/C catalysts reduced with hydrazine hydrate at room temperature (Pd/SnO₂/C-RT) and with hydrogen at 500°C (Pd/SnO₂/C-R500), respectively, were carried out under the same condition. For Pd/SnO₂/C-RT catalysts, the hydrogenation of MA to SAH finished within the first few minutes, which could be ignored compared the whole range of the reaction, and the yields for NBA and GBL were 6.26% and 6.79%, respectively, at 15% SAH conversion. After applying the Pd/SnO₂/C-R500 catalysts, NBA was the primary product with the NBA selectivity increasing to 54.36% at 15% MA conversion due to the existing of SnO₂; SAH (29.64% selectivity) and SA (16% selectivity) were minor products and GBL could not be detected. Namely, the intermediates GBL could hardly accumulated during the hydrogenation of MA since the formed GBL converted to SA completely. This experimental data suggest that the conversion or selectivity of NBA is connected with Pd metal and SnOx species. Dandekar et al. [45] proposed that carbonyl bonds can be adsorbed more strongly on surface Pd-TiOx sites in the case of HTR (high temperature reduction). The O in the C=O groups is assumed to have synergistic effect with either Ti^{x+} at Pd-TiOx sites with the carbon atom coordinated with a neighboring Pd active site, which might lead to a di-σ CO adsorption model. In our case, as mentioned before, the catalyst surface was not only composed of Pd-Sn alloy NPs, but the presence of the metallic state Pd⁰ particles and oxidized states tin species were also observed after the reduction with hydrogen. One could speculate the effect of strong adsorption of inner MA or SAH species by the carbonyl group in di-σ mode on support surface of Pd-SnOx site that was generated by the HTR step (SMSI state) [46-48], increasing the activity and selectivity for hydrogenation of MA to NBA (Scheme 1). A remarkable decrease of activity was also improved by the increase of Sn/Pd ratio from 0.6 to 1.0, which may be interpreted of the intensity adsorption of MA or SAH molecule by the carbonyl group, as a result of the desorption of intermediates becoming increasingly difficult.

The surface alloy composition is changing from Pd₃Sn to Pd₂Sn and Pd₃Sn₂ when the Sn/Pd mass ratios were 0.2, 0.6 and 1, respectively, and the structure of Pd₂Sn is more stable than those of Pd₃Sn and Pd₃Sn₂ [36]. The surface alloy composition of the

catalysts are highly dependent upon the Sn/Pd mass ratios, the corresponding surface active sites govern the reaction activity and selectivity. Therefore, it is feasible to adjust the activity-selectivity relation by tuning the Sn/Pd mass ratios. This part will be calculated by the density functional theory method in our future reports.

3. Conclusion

Pd/C catalysts modified with Sn were used for selective hydrogenation of MA to GBL. The experimental results show that hydrogenation performances of Pd/C catalysts are significantly improved by the presence of Sn. The types of alloy phase and the amounts of the surface Pd-SnO(x) sites altered with Sn/Pd mass ratios from 0–1.0 synthesized in the process of preparation. The maximum reaction rate was 0.57 mol-GBL/(mol-Pd·min) and selectivity was 95.94% when the Sn/Pd mass ratio was 0.6. This might be attributed to that the types of alloy phase and the amount of the surface Pd-SnO_x sites altered with Sn/Pd mass ratios. The catalysts with Pd₂Sn composition alloy and less of Pd-SnO_x sites have higher activity and selectivity of MA to GBL.

4. Experimental

4.1. Catalyst preparation

The impregnations method was used for preparing PdSn(x) (x = 0–1) catalysts with 5 wt% Pd loading. The composition of Pd and Sn were obtained by the precursor of H₂PdCl₄ and Na₂SnO₃, respectively. An aqueous solution of H₂PdCl₄ was prepared by adding PdCl₂ into HCl aqueous solution at room temperature (RT) until PdCl₂ salt was completely dissolved. The active carbon supported Sn-Pd bimetallic catalysts were prepared as follows: the precursor of Na₂SnO₃ and active carbon were charged into deionized water (the ratio of carbon to deionized water was 1 g :10 mL), H₂PdCl₄ solution was injected into the above solution at 353 K. The pH value of slurry was adjusted to 8–9 by dropping a solution of sodium hydroxide (10 wt%), and stirred for 12 h at 353 K. And then, the as-prepared slurry was filtered by deionized water until the pH was about 7, and the wet solid was dried under vacuum for 4 h at 383 K. After that, the samples were calcined under N₂ flow by temperature programming to 773 K at 10 K/min and holding it there for 4h, and followed by reducing under H₂ flow at 723 K for 4 h.

The SnO₂/C were prepared by wetness impregnations of the precursor of SnBu₃Cl, after the slurry was vigorously stirred the pH = 8–9 by aqueous solution of sodium hydroxide. The Pd/SnO₂/C heterogeneous catalysts were synthesis by mixing of H₂PdCl₄ solution and the SnO₂/C to have a 5 wt% Pd loading. And then, the preparation process is the same as Pd/SnO₂/C.

4.2. Characterization techniques

The microstructure and component analysis of the catalysts were characterized by TEM with the attachment of high-angle annular dark-field (HAADF) and energy dispersive X-ray spectroscopy (EDX) (Philips-FEI Tecnai G2 F30 S-Twin). The powder products were dispersed in pure ethanol using ultrasonic cleaner at room temperature for 0.5 h and transferred on carbon-coated copper grids. Average particle sizes were analyzed from at least five different micrographs, and measured at least 100 particles for each samples. XRD measurements of the samples were determined by a PANalytical-X'Pert PRO generator by Cu K α radiation ($\lambda=0.1541$ nm). XPS was determined by a Kratos AXIS Ultra DLD spectrometer. XPS analysis was used the monochromatized aluminum X-ray source and the pass energy of the electron analyzer was 40 eV. The pressure in the catalysts analysis chamber was lower than 6×10^{-9} Torr when at data acquisition. Binding energies (BE) of C1s line was referred to at 284.8 eV.

4.3. Liquid-phase Hydrogenation of MA to GBL

Hydrogenation of MA to GBL was carried through as follows: 0.3 g catalyst, 5.0 g MA and 200 mL dioxane were put into a 500 mL steel autoclave. The air in reactor was filled with N₂ three times, followed by replacing N₂ by H₂ for three times. The reaction was started immediately after the autoclave heated slowly to 433 K, and the hydrogen pressure setting to 5.0 MPa. In order to eliminate the effects of external diffusion, the stirring rate was set as 900 rpm. Gas chromatography was used to analysis the reaction progress, and at different time intervals \sim 0.50 mL reaction liquid was monitored. The selectivity of hydrogenation of MA, is defined as:

$$\text{GBL Selectivity} = \frac{\text{GBL}\%}{\text{GBL}\% + \text{SAH}\% + \text{SA}\% + \text{THF}\% + \text{BA}\% + \text{BD}\%} \times 100\%$$

where MA, SA, SAH, GBL, BA, NBA, THF, and BD represent the amount of maleic anhydride, succinic acid, succinic anhydride, γ -butyrolactone, *n*-butyric acid, *n*-butyl alcohol, tetrahydrofuran, and butanediol in the mixture.

Acknowledgment

The project was supported by the National Natural Science Foundation, China (Nos. 21506138, 21606199, 21575097 and 21375092), the Natural Science Foundation of Zhejiang Province, China (No. LQ15B060001) and the China Postdoctoral Science Foundation (No. 2016M592015).

References

- [1] Y. Zou, Y. Leng, C. Huang, et al., Measurement and correlation of solubility of succinic anhydride in pure solvents and binary solvent mixtures, *J. Chem. Thermodyn.* 104 (2017) 82-90.
- [2] L.F. Chen, P.J. Guo, L.J. Zhu, et al., Preparation of Cu/SBA-15 catalysts by different methods for the hydrogenolysis of dimethyl maleate to 1,4-butanediol, *Appl. Catal. A* 356 (2009) 129-136.
- [3] N. Harris, M.W. Tuck, Butanediol *via* maleic anhydride, *Hydrocarbon Process* 69 (1990) 79-82.
- [4] B. Intra, J. Euanorasetr, T. Nihira, et al., Characterization of a gamma-butyrolactone synthetase gene homologue (*stcA*) involved in bafilomycin production and aerial mycelium formation in *Streptomyces* sp. SBI034, *Appl. Microbiol. Biotechnol.* 100 (2016) 2749-2760.
- [5] A.M. Brownstein, 1,4-butanediol and tetrahydrofuran: exemplary small-volume commodities. *Chem. Tech.* 21 (1991) 506-510.
- [6] U.G. Hong, J.K. Kim, J. Lee, et al., Song, Hydrogenation of succinic acid to tetrahydrofuran (THF) over ruthenium-carbon composite (Ru-C) catalyst, *Appl. Catal. A* 469 (2014) 466-471.
- [7] Y. Huang, Y. Ma, Y. Cheng, et al., Active ruthenium catalysts prepared by cacumen platycladi leaf extract for selective hydrogenation of maleic anhydride, *Appl. Catal. A* 495 (2015) 124-130.
- [8] Y. Ma, Y. Huang, Y. Chen, et al., Selective liquid-phase hydrogenation of maleic anhydride to succinic anhydride on biosynthesized ru-based catalysts, *Catal. Commun.* 57 (2014) 40-44.
- [9] B. Zhang, Y. Zhu, G. Ding, et al., Modification of the supported Cu/SiO₂ catalyst by alkaline earth metals in the selective conversion of 1,4-butanediol to γ -butyrolactone, *Appl. Catal. A* 443-444 (2012) 191-201.
- [10] M.E. Bertone, S.A. Regenhardt, C.I. Meyer, et al., Highly selective Cu-modified Ni/SiO₂-Al₂O₃ catalysts for the conversion of maleic anhydride to γ -butyrolactone in gas phase, *Top. Catal.* 59 (2016) 1-9.
- [11] D. Zhang, H. Yin, J. Xue, et al., Selective hydrogenation of maleic anhydride to tetrahydrofuran over Cu-Zn-M (M = Al, Ti, Zr) catalysts using ethanol as a solvent, *Ind. Eng. Chem. Res.* 48 (2009) 11220-11224.
- [12] H.P.R. Kannapu, C.K.P. Neeli, K.S.R. Rao, et al., Unusual effect of cobalt on Cu-MgO catalyst for the synthesis of γ -butyrolactone and aniline via coupling reaction, *Catal. Sci. Technol.* 6 (2016) 5494-5503.
- [13] D. Zhang, H. Yin, C. Ge, et al., Selective hydrogenation of maleic anhydride to γ -butyrolactone and tetrahydrofuran by Cu-Zn-Zr catalyst in the presence of ethanol, *J. Ind. Eng. Chem.* 15 (2009) 537-543.
- [14] S.A. Regenhardt, C.I. Meyer, T.F. Garetto, et al., Selective gas phase hydrogenation of maleic anhydride over Ni-supported catalysts: Effect of support on the catalytic performance, *Appl. Catal. A* 449 (2012) 81-87.
- [15] M.E. Bertone, C.I. Meyer, S.A. Regenhardt, et al., Highly selective conversion of maleic anhydride to γ -butyrolactone over Ni-supported catalysts prepared by precipitation-deposition method, *Appl. Catal. A* 503 (2015) 135-146.
- [16] J. Li, W. Tian, L. Shi, Hydrogenation of maleic anhydride to succinic anhydride over Ni/HY-Al₂O₃, *Ind. Eng. Chem. Res.* 49 (2010) 11837-11840.
- [17] J. Li, W.P. Tian, X. Wang, et al., Nickel and nickel-platinum as active and selective catalyst for the maleic anhydride hydrogenation to succinic anhydride, *Chem. Eng. J.* 175 (2011) 417-422.
- [18] S. Wei, C. Pan, X. Yang, et al., Coupling reaction of 1,4-butanediol with maleic anhydride over Cr-Cu/SiO₂ catalysts, *Acta Chim. Sinica* 66 (2008) 1287.
- [19] S. Li, X. Wang, X. Liu, et al., Aqueous-phase hydrogenation of biomass-derived itaconic acid to methyl- γ -butyrolactone over Pd/C catalysts: Effect of pretreatments of active carbon, *Catal. Commun.* 61 (2015) 92-96.
- [20] C. Zhang, L. Chen, H. Cheng, et al., Atomically dispersed Pd catalysts for the selective hydrogenation of succinic acid to γ -butyrolactone, *Catal. Today* 276 (2016) 55-61.
- [21] Z. Jin, C. Yu, X. Wang, et al., Liquid phase hydrodechlorination of chlorophenols at lower temperature on a novel Pd catalyst, *J. Hazard. Mater.* 186 (2011) 1726-1732.

- [22] F.D. Kopinke, D. Angeles-Wedler, D. Fritsch, et al., Pd-catalyzed hydrodechlorination of chlorinated aromatics in contaminated waters-Effects of surfactants, organic matter and catalyst protection by silicone coating, *Appl. Catal. B Environ.* 96 (2010) 323-328.
- [23] H. Rong, S. Cai, Z. Niu, et al., Composition-dependent catalytic activity of bimetallic nanocrystals: AgPd-catalyzed hydrodechlorination of 4-chlorophenol, *ACS Catal.* 3 (2013) 1560-1563.
- [24] U.R. Pillai, E. Sahle-Demessie, ChemInform Abstract: selective hydrogenation of maleic anhydride to γ -butyrolactone over Pd/Al₂O₃ catalyst using supercritical CO₂ as solvent, *Chem. Commun.* 33 (2002) 422-423.
- [25] U.R. Pillai, E. Sahle-Demessie, D. Young, Maleic anhydride hydrogenation over Pd/Al₂O₃ catalyst under supercritical CO₂ medium, *Appl. Catal. B* 43 (2003) 131-138.
- [26] S.H. Vaidya, C.V. Rode, R.V. Chaudhari, Bimetallic Pt-Sn/ γ -alumina catalyst for highly selective liquid phase hydrogenation of diethyl succinate to γ -butyrolactone, *Catal. Commun.* 8 (2007) 340-344.
- [27] S. Furukawa, M. Endo, T. Komatsu, Bifunctional catalytic system effective for oxidative dehydrogenation of 1-butene and *n*-Butane using Pd-based intermetallic compounds, *ACS Catal.* 4 (2014) 3533-3542.
- [28] O. Lidor-Shalev, D. Zitoun, Reaction mechanism of "Amine-Borane Route" towards Sn, Ni, Pd, Pt nanoparticles, *RSC Adv.* 4 (2014) 63603-63610.
- [29] E. Esmaeili, Y. Mortazavia, A.A. Khodadadi, et al., The role of tin-promoted Pd/MWNTs *via* the management of carbonaceous species in selective hydrogenation of high concentration acetylene, *Appl. Surf. Sci.* 263 (2012) 513-522.
- [30] E. Esmaeili, A.M. Rashidi, A.A. Khodadadi, et al., Palladium-tin nanocatalysts in high concentration acetylene hydrogenation: A novel deactivation mechanism, *Fuel Process. Technol.* 120 (2014) 113-122.
- [31] W. Du, K.E. Mackenzie, D.F. Milano, et al., Palladium-tin alloyed catalysts for the ethanol oxidation reaction in an alkaline medium, *ACS Catal.* 2 (2012) 287-297.
- [32] J. Zhao, X. Xu, X. Li, et al., Promotion of Sn on the Pd/AC catalyst for the selective hydrogenation of cinnamaldehyde, *Catal. Commun.* 43 (2014) 102-106.
- [33] S.M. Jung, E. Godard, S.Y. Jung, et al., Liquid-phase hydrogenation of maleic anhydride over Pd-Sn/SiO₂, *Catal. Today* 87 (2003) 171-177.
- [34] E. Esmaeili, Y. Mortazavi, A.A. Khodadadi, et al., The role of tin-promoted Pd/MWNTs *via* the management of carbonaceous species in selective hydrogenation of high concentration acetylene, *Appl. Surf. Sci.* 263 (2012) 513-522.
- [35] R.M. Modibedi, T. Masombuka, M.K. Mathe, Carbon supported Pd-Sn and Pd-Ru-Sn nanocatalysts for ethanol electro-oxidation in alkaline medium, *J. Hydrogen Energy* 36 (2001) 4664-4672.
- [36] A.F. Lee, C.J. Baddeley, M.S. Tikhov, et al., Structural and electronic properties of Sn overlayers and Pd/Sn surface alloys on Pd(111), *Surf. Sci.* 373 (1997) 195-209.
- [37] K. Kovnir, J. Osswald, M. Armbrüster, et al., Etching of the intermetallic compounds PdGa and Pd₃Ga₇: An effective way to increase catalytic activity, *J. Catal.* 264 (2009) 93-103.
- [38] K. Kovnir, M. Armbrüster, D. Teschner, et al., A new approach to well-defined, stable and site-isolated catalysts, *Sci. Technol. Adv. Mater.* 8 (2007) 420-427.
- [39] D. Teschner, A. Pestryakov, E. Kleimenov, et al., High-pressure X-ray photoelectron spectroscopy of palladium model hydrogenation catalysts. Part 1: Effect of gas ambient and temperature, *J. Catal.* 230 (2005) 186.
- [40] D. Teschner, A. Pestryakov, E. Kleimenov, et al., High-pressure X-ray photoelectron spectroscopy of palladium model hydrogenation catalysts. Part 2: Hydrogenation of trans -2-pentene on palladium, *J. Catal.* 230 (2005) 195-203.
- [41] S.M. Jung, E. Godard, S.Y. Jung, et al., Liquid-phase hydrogenation of maleic anhydride over Pd-Sn/SiO₂, *Catal. Today.* 87 (2003) 171-177.
- [42] E.A. Sales, J. Jove, M.J. Mendes, et al., Palladium, palladium-tin, and palladium-silver catalysts in the selective hydrogenation of hexadienes: TPR, mössbauer, and infrared studies of adsorbed CO, *J. Catal.* 195 (2000) 88-95.
- [43] I.M. J. Vilella, S.R. deMiguel, O.A. Scelza, Pt, PtSn and PtGe catalysts supported on granular carbon for fine chemistry hydrogenation reactions, *J. Mol. Catal. A* 284 (2008) 161-171.
- [44] A. Haghofer, K. Föttinger, F. Girgsdies, et al., In situ study of the formation and stability of supported Pd₂Ga methanol steam reforming catalysts, *J. Catal.* 286 (2012) 13-21.
- [45] A. Dandekar, M.A. Vannice, Crotonaldehyde Hydrogenation on Pt/TiO₂ and Ni/TiO₂ SMSI Catalysts, *J. Catal.* 183 (1999) 344-354.
- [46] S.J. Tauster, S.C. Fung, R.L. Garten, ChemInform abstract: strong metal-support interactions. group 8 noble metals supported in titanium dioxide, *J. Am. Chem. Soc.* 100 (1978) 170-175.
- [47] J.K.A. Clarke, R.J. Dempsey, T. Baird, et al., Selectivities for hydrocarbon reactions on SMSI titania-supported platinum formed by high-temperature reduction, *J. Catal.* 126 (1990) 370-380.
- [48] S.J. Tauster, S.C. Fung, Strong metal-support interactions: Occurrence among the binary oxides of groups IIA-VB, *J. Catal.* 55 (1978) 29-35.

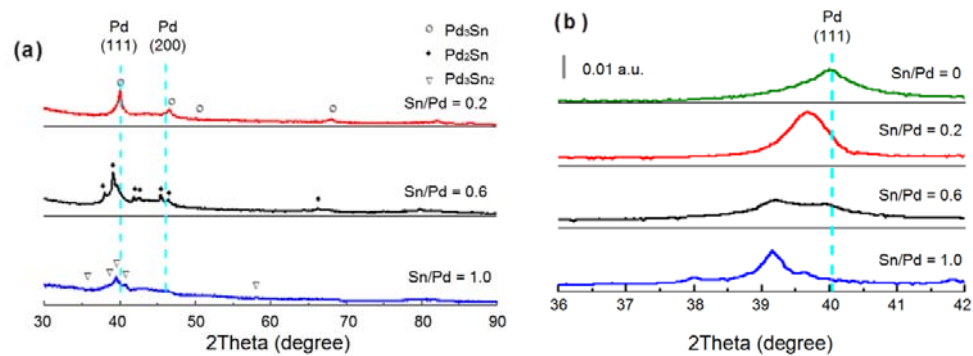


Fig. 1 (a) XRD patterns of PdSn(x) catalysts, $x = \text{Sn/Pd}$; (b) The magnified peaks of the PdSn(x) catalyst.

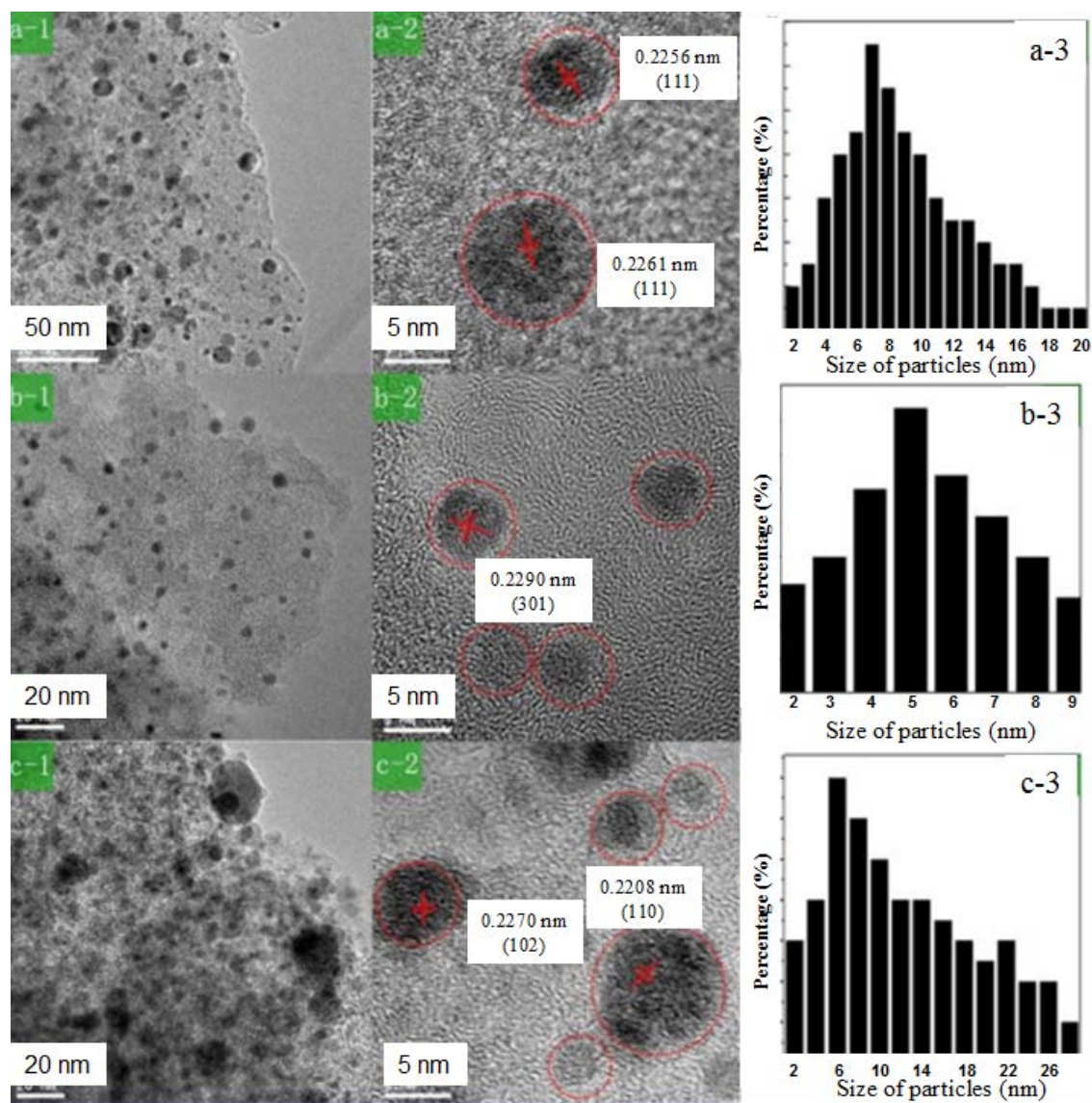


Fig. 2 TEM results for PdSn(x) catalysts: a, $x = 0.2$; b, $x = 0.6$; c, $x = 1.0$.

1, Low-resolution TEM images; 2, high-resolution TEM images; 3, corresponding size distribution.

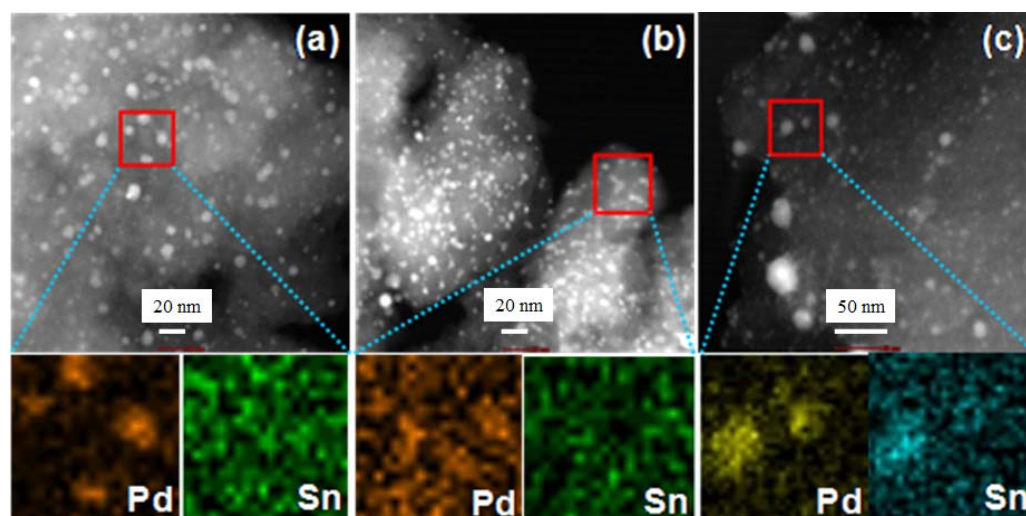


Fig. 3 The HETEM images and the corresponding mapping energy dispersive X-ray spectroscopy (EDX) intensity profiles of PdSn(x) catalysts of (a) $x = 0.2$; (b) $x = 0.6$; (c) $x = 1.0$.

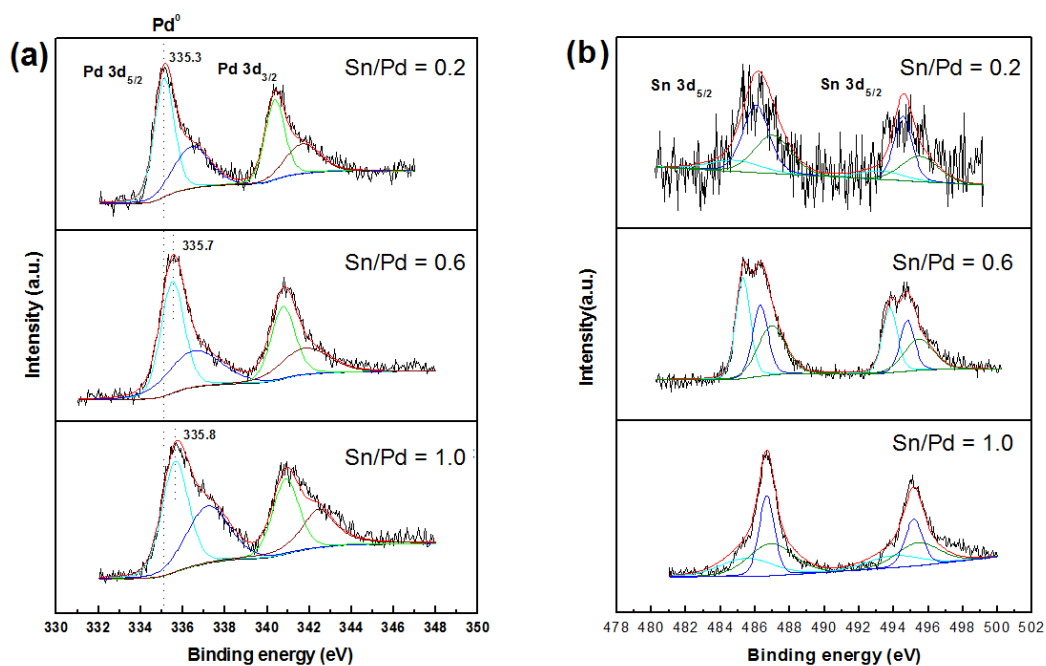
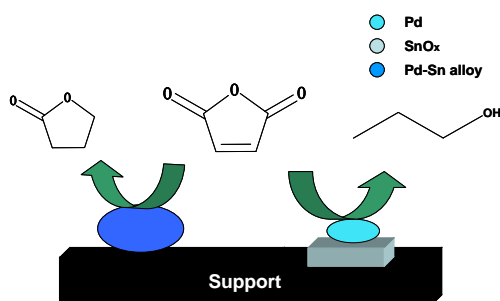


Fig. 4. XP spectra of Pd 3d (a) and Sn 3d (b) of PdSn(x) catalysts.



Scheme1. Schematic representation of Pd/C modified with Sn catalyst for liquid-phase selective hydrogenation of maleic anhydride to gamma-butyrolactone.

Table 1

The binding energy (eV) of Pd 3d5/2 and Sn 3d5/2 and relative percentage of surface species for the PdSn(x) catalysts.

Sn/Pd mass ratio	0.2	0.6	1.0
Metal Pd ⁰ 3d5/2 (eV)	335.3	335.7	335.8
(FWHM)	1.12	1.43	1.50
Intermetallic Pd ⁰ 3d5/2 (eV)	336.7	336.7	337.4
Metal Pd ⁰ / Pd _{total}	0.54	0.55	0.56
Sn ⁰ 3d5/2 (eV)	484.8	485.2	485.5
Sn ²⁺ 3d5/2 (eV)	486.1	486.3	486.6
Sn ⁴⁺ 3d5/2 (eV)	487.0	487.1	486.9
Sn ⁰ /Sntotal	0.15	0.24	0.28
Sn ⁰ /[Sn ⁰ + intermetallic Pd ⁰]	0.25≈Pd ₃ Sn	0.34≈Pd ₂ Sn	0.39≈Pd ₃ Sn ₂

Table 2

The catalytic activities and selectivity of PdSn(x) catalysts in the hydrogenation of MA.

Catalyst	Rate ^a	THF (%)	BD (%)	SAH (%)	BA (%)	NBA (%)	SA (%)	GBL (%)
PdSn(0)	0.03	0.32	0	35.07	0.15	12.66	2.08	49.73
PdSn(0.2)	0.05	0	0	0	0.06	6.83	3.21	89.90
PdSn(0.6)	0.57	0	0	0	0	2.57	1.49	95.94
PdSn(1.0)	0.09	0	0	0	0.15	10.13	3.81	85.91

^a rate = mol-GBL/(mol-Pd·min), reaction temperature = 160 °C, reaction pressure = 5 MPa, conversion = 100%.